AGU ADVANCING EARTH AND SPACE SCIENCE

Geophysical Research Letters

RESEARCH LETTER
10.1029/2020GL089235

Linearity of Outgoing Longwave Radiation: From an Atmospheric Column to Global Climate Models

Yi Zhang[1], Nadir Jeevanjee[2], and Stephan Fueglistaler[1,3]

[1]Program in Atmospheric and Oceanic Sciences, Princeton University, Princeton, NJ, USA, [2]NOAA/Geophysical Fluid Dynamics Laboratory, Princeton, NJ, USA, [3]Department of Geosciences, Princeton University, Princeton, NJ, USA

Key Points:
- The longwave clear-sky (LWCS) feedback has diverse spatial patterns in CMIP5 models, yet the global-mean feedback is robustly 1.9 W/m^2/K
- The diverse spatial patterns of LWCS feedback across models can be explained by their spatial patterns of column RH changes
- The robustness of the global-mean LWCS feedback results from OLR being linear when conditioned upon RH and the invariance of the RH histogram

Supporting Information:
- Supporting Information S1

Correspondence to:
Y. Zhang,
yz8@princeton.edu

Citation:
Zhang, Y., Jeevanjee, N., & Fueglistaler, S. (2020). Linearity of outgoing longwave radiation: From an atmospheric column to global climate models. *Geophysical Research Letters*, *47*, e2020GL089235. https://doi.org/10.1029/2020GL089235

Received 8 JUN 2020
Accepted 20 AUG 2020
Accepted article online 25 AUG 2020

Abstract The linearity of global-mean outgoing longwave radiation (OLR) with surface temperature is a basic assumption in climate dynamics. This linearity manifests in global climate models, which robustly produce a global-mean longwave clear-sky (LWCS) feedback of 1.9 W/m^2/K, consistent with idealized single-column models (Koll & Cronin, 2018, https//:doi.org/10.1073/pnas.1809868115). However, there is considerable spatial variability in the LWCS feedback, including negative values over tropical oceans (known as the "super-greenhouse effect") which are compensated for by larger values in the subtropics/extratropics. Therefore, it is unclear how the idealized single-column results are relevant for the global-mean LWCS feedback in comprehensive climate models. Here we show with a simple analytical theory and model output that the compensation of this spatial variability to produce a robust global-mean feedback can be explained by two facts: (1) When conditioned upon free-tropospheric column relative humidity (RH), the LWCS feedback is independent of RH, and (2) the global histogram of free-tropospheric column RH is largely invariant under warming.

Plain Language Summary In response to CO_2 forcing, the Earth's climate warms and emits more outgoing longwave radiation (OLR) to space. This OLR emission is linear with the global-mean surface temperature as a result of the water vapor feedback. Previous work has demonstrated this understanding in single-column atmospheric models with fixed relative humidity (RH). The question remains, however, why the Earth behaves like a single atmospheric column given the diversity of RH values across the globe. Here we theoretically show that the analog for fixed RH of a single column is that the global RH histogram is invariant under warming. We further demonstrate with model output that this invariance indeed holds. These results thus fill the missing link between single-column theory and the fact that global-mean OLR is linear in surface temperature.

1. Introduction

A standard paradigm for analyzing the Earth's climate and climate sensitivity is to treat the climate as a linear system (e.g., Gregory et al., 2004). An implicit assumption in such treatments is that the global-mean outgoing longwave radiation (OLR) is linear in global-mean surface temperature ($\overline{T_s}$). Indeed, as is shown in Figure 1a, the annual-mean global-mean clear-sky OLR ($\overline{\mathrm{OLR}}$) from the Coupled Model Intercomparison Project phase 5 (CMIP5) (Taylor et al., 2012) increases in a strikingly linear fashion with $\overline{T_s}$ for each model after abruptly quadrupling CO_2 concentration. Though models warm by various amounts after 150 years, the longwave clear-sky (LWCS) feedback (slope of the linear regression of $\overline{\mathrm{OLR}}$ against $\overline{T_s}$) varies by only 5% around the mean value of 1.88 W/m^2/K for the nine models from different modeling centers shown, consistent with previous work (Andrews et al., 2015). Notably, this value is also consistent with the idealized single-column model calculations by Koll and Cronin (2018) over a wide range of surface temperatures.

This robust global-mean LWCS feedback, however, is made up of nonuniform local responses which moreover differ among models. The OLR increase per unit warming in the deep tropics is relatively low, and sometimes even negative, an effect known as the "super-greenhouse effect." This phenomenon has received some attention as a local feedback (Dewey & Goldblatt, 2018; Raghuraman et al., 2019; Raval & Ramanathan, 1989; Stephens & Greenwald, 1991; Stephens et al., 2016; Valero et al., 1997), but its relevance for global climate sensitivity is unclear given that other regions seem to emit *more* OLR per unit warming to compensate. Here we would like to understand this compensation and whether it is guaranteed under global warming.

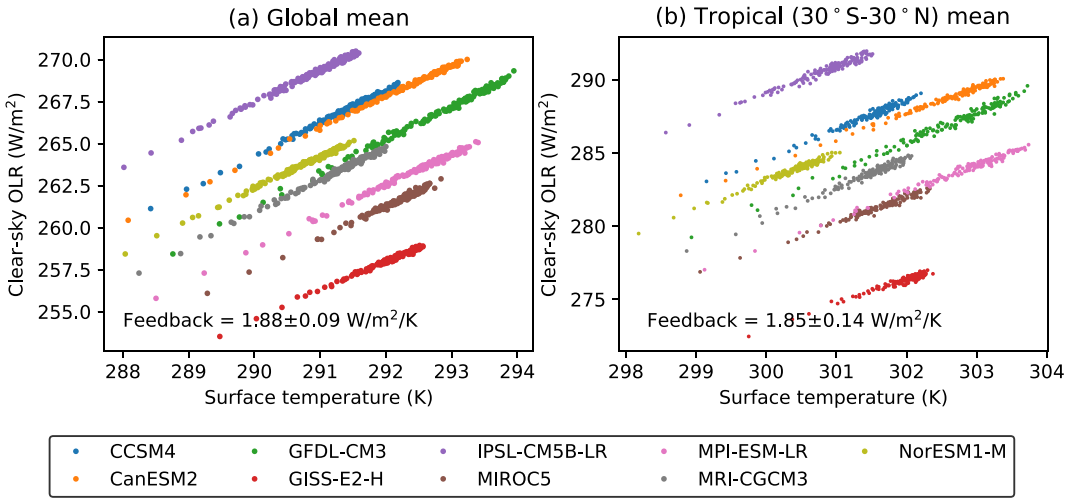

Figure 1. (a) Annual mean and global-mean clear-sky OLR versus global-mean surface temperature of CMIP5 models for the abrupt 4xCO_2 experiment. (b) The same as panel (a) but for the tropical (30°S to 30°N) mean.

The origin of OLR being linear in T_s rather than quartic (as suggested by the Stefan-Boltzmann law) lies in the water vapor feedback at fixed relative humidity (RH) (Held & Shell, 2012; Ingram, 2010; Koll & Cronin, 2018). OLR calculations with a single-column model at fixed RH and moist-adiabatic temperature profiles indeed confirm that there exists a wide range of T_s where the LWCS feedback varies by less than ±10% around 2.2 W/m^2/K (Koll & Cronin, 2018). Here we summarize these results with the following equation:

$$\left.\frac{\partial \mathrm{OLR}}{\partial T_s}\right|_{\mathrm{RH}} \approx \alpha \approx 2\,\mathrm{W/m^2/K}. \tag{1}$$

However, unlike these idealized column models, the vertical profile of RH in realistic atmospheres is rarely uniform, and inversions can complicate the vertical temperature profiles. Furthermore, the RH profile in a given column need not be constant, as previous studies have found that the geographical distribution of RH is strongly affected by the atmospheric circulation, which affects the local OLR-T_s relationship (Allan et al., 1999; Held & Soden, 2000; Raval et al., 1994). Therefore, Equation 1 is not directly applicable to the global-mean of CMIP5 models shown in Figure 1a. Although Koll and Cronin (2018) assess Equation 1 using global satellite data, that data only probes spatial variations in T_s rather than the global-mean feedback under global warming. It is thus unclear whether the agreement in LWCS feedback between global climate models and idealized single-column models is coincidental.

Here we show that this agreement is not a coincidence. We first investigate the spatial patterns of LWCS feedback in CMIP5 models to get a sense of how the spatial patterns compensate, and further show that these spatial patterns are tied to column RH changes. We find that α is independent of column RH so long as the column RH is interpreted as being in the free troposphere. We then show analytically that the global-mean LWCS feedback will be equal to α so long as the global histogram of column RH doesn't change with warming, a criterion satisfied to a large degree by all CMIP5 models.

2. Materials and Methods

The LWCS feedback is diagnosed following the forcing-response analysis introduced by Gregory et al. (2004). Monthly mean output of global climate models from CMIP5 (Taylor et al., 2012) for the abrupt 4xCO_2 experiment (abruptly quadrupling CO_2 then integrating for 150 years) is analyzed. The local LWCS feedback is determined by linear regression of local clear-sky OLR onto *local* surface temperature to emphasize the physical connection between OLR and local surface temperature (Feldl & Roe, 2013), which is not the same as earlier work that regresses local radiative quantities onto global-mean surface temperature (e.g., Andrews et al., 2015; Stephens et al., 2016). As the clear-sky feedback is roughly constant throughout the entire

length of the simulation (150 years; Figure 1), we will not separate the fast response epoch (the first 20 years or so) and the slow response epoch (the remaining 130 years or so) in the following analysis.

Column RH is calculated as the water vapor mass divided by the saturated water vapor mass within the column. To calculate the water vapor mass between every two pressure levels, specific humidity data are interpolated to the center of pressure levels assuming linearity with the logarithm of pressure and then weighted by the pressure difference between every two levels. The upper boundary for column RH calculation is chosen to be 300 hPa. Ideally, the tropopause is the upper boundary for the column, but considering the limited output levels of CMIP5 models, this choice is made to include as much of the tropospheric water vapor as possible while also being sure to exclude the stratosphere. We do this because neglecting the water vapor between 300 hPa and the tropopause makes little difference to column RH due to the very low temperatures there, while contamination from the stratosphere can bias the saturated water vapor mass due to the higher temperatures in the stratospheric inversion.

3. Spatial Pattern of LWCS Feedback and Connection to Column RH

We demonstrate the spatial pattern of the LWCS feedback and the ensuing compensation which produces the robust value of α shown in Figure 1a by gradually increasing the spatial dimensions of our analysis. Figure 2a shows the zonal-mean feedback obtained by regressing the zonal-mean clear-sky OLR onto the zonal-mean surface temperature using decadal mean data (to smooth over interannual internal variability). The zonal-mean LWCS feedback is not uniform across latitudes, with a minimum of 1 $W/m^2/K$ in the deep tropics and a typical value of 2 $W/m^2/K$ in the extratropics in the multimodel mean. The linearity of clear-sky OLR with T_s can be assessed by the R^2 of the local OLR-T_s linear regression. The linearity is remarkably strong in the extratropics, indicated by the close to 100% of explained variance (Figure 2b), and somewhat weaker in the tropics. Models also tend to agree better in the extratropics as measured by the standard deviation of LWCS feedback (Figure 2c).

Figure 2d shows the map of LWCS feedback. In the extratropics, similar to the zonal mean (Figure 2a), the LWCS feedback is relatively spatially uniform and lacks any land-ocean contrast. In the tropics, however, regions of negative feedback emerge, which is the "super-greenhouse effect" referred to in section 1. The linearity is again remarkably strong in the extratropics for each location but is weak within the 30°S to 30°N latitude band (Figure 2e). Models show very good agreement of the LWCS feedback in the extratropics, while in the tropics, the standard deviation across models is of the same magnitude as the feedback itself in the tropics (Figure 2f), consistent with previous findings that models disagree on the locations and strengths of "super-greenhouse effect" (Stephens et al., 2016).

To understand the spatial pattern and the model spread of the LWCS feedback shown in Figure 2, we consider the joint dependence of OLR on T_s and RH. Invoking Equation 1 but also allowing for RH changes with warming yields

$$\frac{\mathrm{d\ OLR}}{\mathrm{d}T_s} = \alpha + \beta \frac{\mathrm{dRH}}{\mathrm{d}T_s}, \tag{2}$$

where $\beta = \frac{\partial \mathrm{OLR}}{\partial \mathrm{RH}}\big|_{T_s}$. Equation 2 indicates that the spatial pattern of the LWCS feedback should be closely related to the spatial pattern of $\frac{\mathrm{dRH}}{\mathrm{d}T_s}$. A similar idea is mentioned in Held and Soden (2000). In testing this idea, we begin by using column RH and later refine this by using the free-tropospheric column RH.

Figure 3 illustrates the accuracy of Equation 2 with two models that feature different patterns of LWCS feedback. In GFDL-CM3, the regions of super-greenhouse effect are mainly located in the equatorial West Pacific, while in CCSM4, these regions expand off equator and are mainly located in the central Pacific. For both models, the spatial patterns of LWCS feedback (color shading) and the column RH changes (contours) are almost identical (Figures 3a and 3c). To make this more explicit, we plot $\frac{\mathrm{d\ OLR}}{\mathrm{d}T_s}$ versus $\frac{\mathrm{dRH}}{\mathrm{d}T_s}$ in Figures 3b and 3d, taking only grid points within 30°S to 30°N. The correlations for GFDL-CM3 and CCSM4 are −0.89 and −0.93, respectively, and −0.87 for all the nine CMIP5 models in Figure 1 on average. Moreover, the y-intercept of the linear regression is on average 1.9 $W/m^2/K$, which

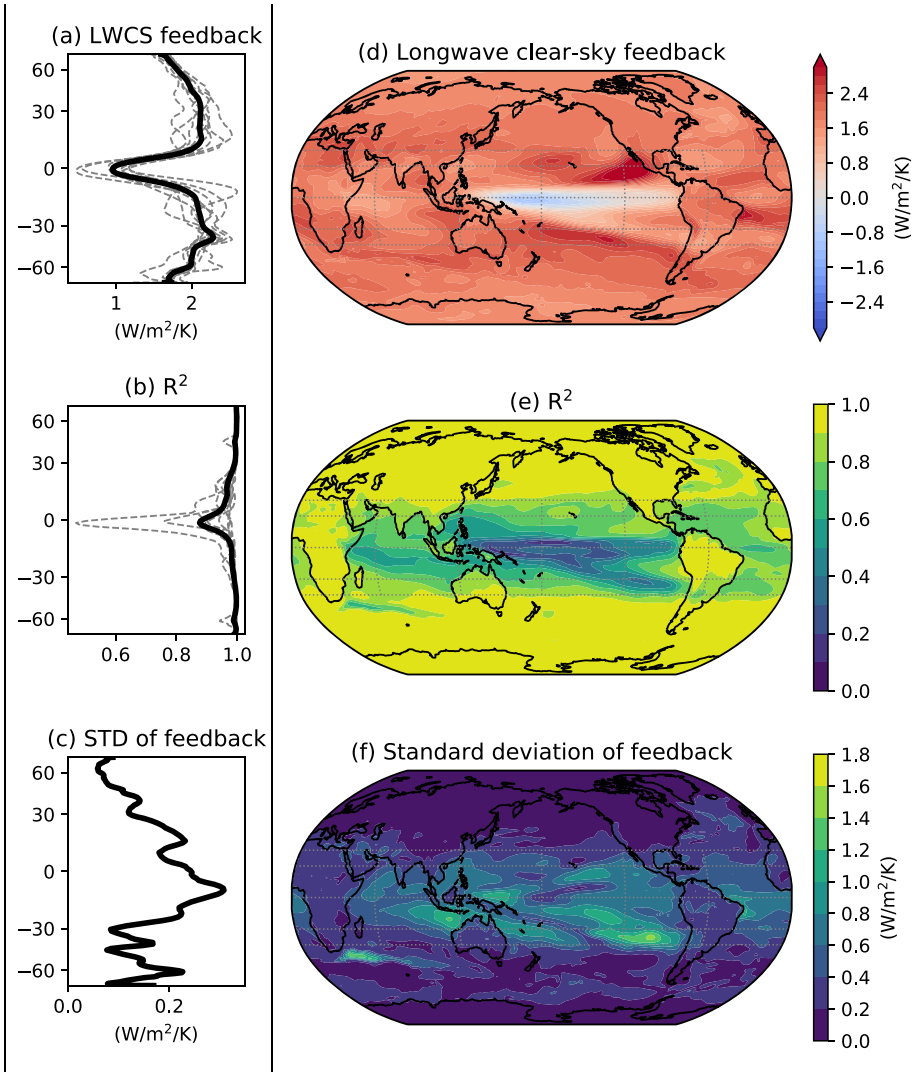

Figure 2. (a) Zonal-mean LWCS feedback for each model (dashed) and the multimodel mean (solid). (b) The R^2 of the linear regression of zonal-mean OLR onto the zonal-mean T_s for each model (dashed) and the multimodel mean (solid). (c) Standard deviation of the zonal-mean LWCS feedback among models. Panels (d), (e), and (f) show the same variables as in panels (a), (b), and (c), respectively, on 2-D maps.

indeed recovers the value of α (see Figures 3b and 3d for GFDL-CM3 and CCSM4). In other words, for locations where column RH doesn't change with warming, the LWCS feedback is close to the value given by Equation 1.

A key feature of Figures 3a and 3c is that column RH increases in the deep tropics are accompanied by column RH decreases in the subtropics. This implies that the local effects of RH changes on OLR might cancel out in the global mean or even just in the tropical mean as indeed seen in Figure 1b. This suggests that the robustness of the global-mean LWCS feedback evident in Figure 1 results from a geographical *rearrangement* of column RH values, without any change in the column RH histogram. We test these ideas in section 5, but first we return to the question of to what extent Equation 1 applies to realistic atmospheres with nonuniform RH profiles.

4. OLR-T_s Relationship Conditioned Upon Column RH

Equation 1, a central result of (Koll & Cronin, 2018), was tested in an idealized single column atmospheric model with vertically uniform RH profiles and moist adiabatic temperature profiles. However, we know that

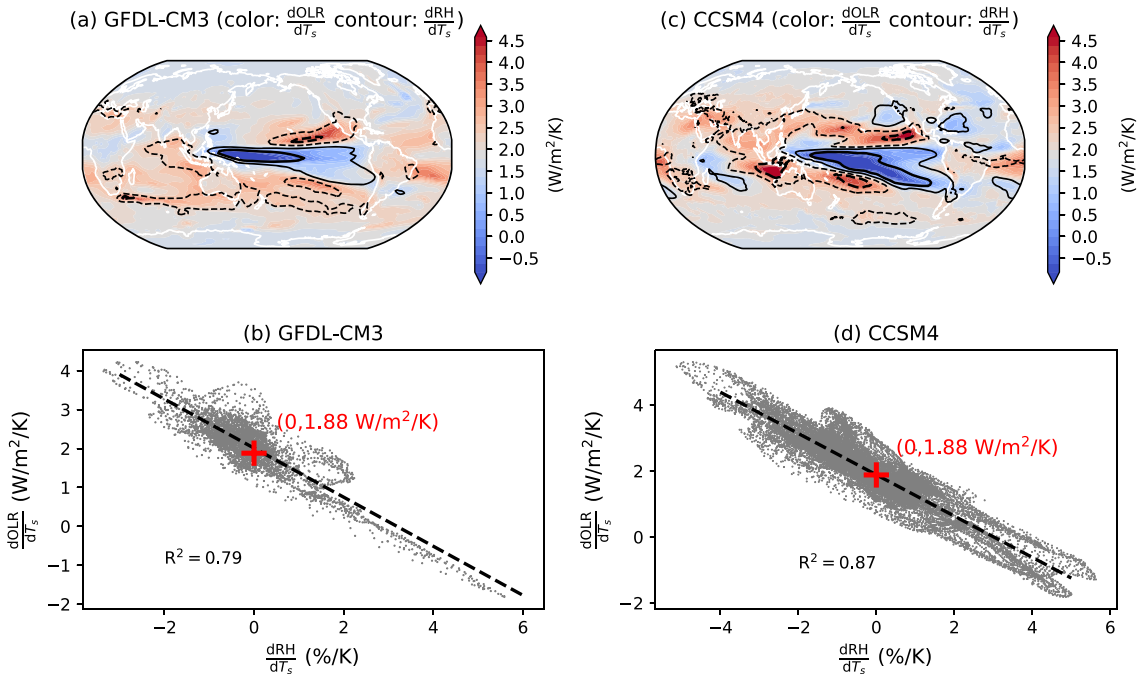

Figure 3. (a) Location-specific longwave clear-sky feedback parameters (color shading) and the sensitivity of column relative humidity (RH) to surface temperature (black contours) for GFDL-CM3. Contours of −3%/K (thick dashed), −1%/K (thin dashed), 1%/K (thin solid), and 3%/K (thick solid) are shown. (b) Scatter plot of the two fields shown in panel (a) and the linear regression line. The red cross marks the point of zero column RH change and a LWCS feedback of 1.88 W/m^2/K. Panels (c) and (d) are the same as panels (a) and (b), but for CCSM4.

the real atmosphere exhibits more complicated vertical structures of temperature and RH, which influence the OLR (Huang et al., 2007; Shine & Sinha, 1991).

To test the applicability of Equation 1 to more realistic atmospheres, Figure 4a shows the OLR dependence on T_s conditioned upon various column RH ranging from 40% to 70%. As expected, the OLR increases as column RH decreases for a given T_s. Furthermore, at relatively low T_s, the slope (the LWCS feedback) is around 1.9 W/m^2/K for all column RH values, consistent with Equation 1. However, OLR decreases with T_s at T_s above 303 K, which is inconsistent with Equation 1. Although a flattening of OLR-T_s curve is expected from the closing of the water vapor window (Koll & Cronin, 2018), this happens at a much higher temperature and cannot explain the *decrease* of OLR with T_s seen here. This decrease of OLR with T_s is distinct from the super-greenhouse effect discussed above because here it occurs even at fixed column RH.

What then causes this breakdown of Equation 1 in realistic atmospheric columns? A single column RH is insufficient for representing the vertical structure of water vapor in realistic climate models, as the boundary-layer RH (Byrne & O'Gorman, 2016; Held & Soden, 2000) and the free-tropospheric RH (Galewsky et al., 2005; Pierrehumbert, 1998; Pierrehumbert & Roca, 1998; Romps, 2014) are determined by essentially independent processes which are sometimes decoupled. Furthermore, it is known that in contrast to the upper troposphere, the influence of the boundary-layer RH on OLR is quite weak (Soden & Held, 2006; Soden et al., 2008). Physically, this is because the boundary-layer air temperature is close to T_s, and an increase in the emission from the boundary-layer water vapor is approximately equal to the decrease in surface emission. To strengthen this point, we conduct experiments with PyRADS, a line-by-line radiation code, of varying free-tropospheric and boundary-layer RH separately under fixed T_s at 288 K (roughly equal to the present day global-mean temperature). We find that even though the total water vapor path above 850 hPa is only 1.4 times of that below 850 hPa, the OLR responses of the former is 17 times of that of the latter (Figure S1 in the supporting information). This suggests that we should focus on free-tropospheric RH rather than boundary-layer RH. Figure 4d shows the same OLR-T_s relationship as in Figure 4a but now conditioned on the free-tropospheric (300–850 hPa) column RH. With this RH variable, the decrease in OLR with T_s at higher T_s disappears, and Equation 1applies for most RH and T_s values.

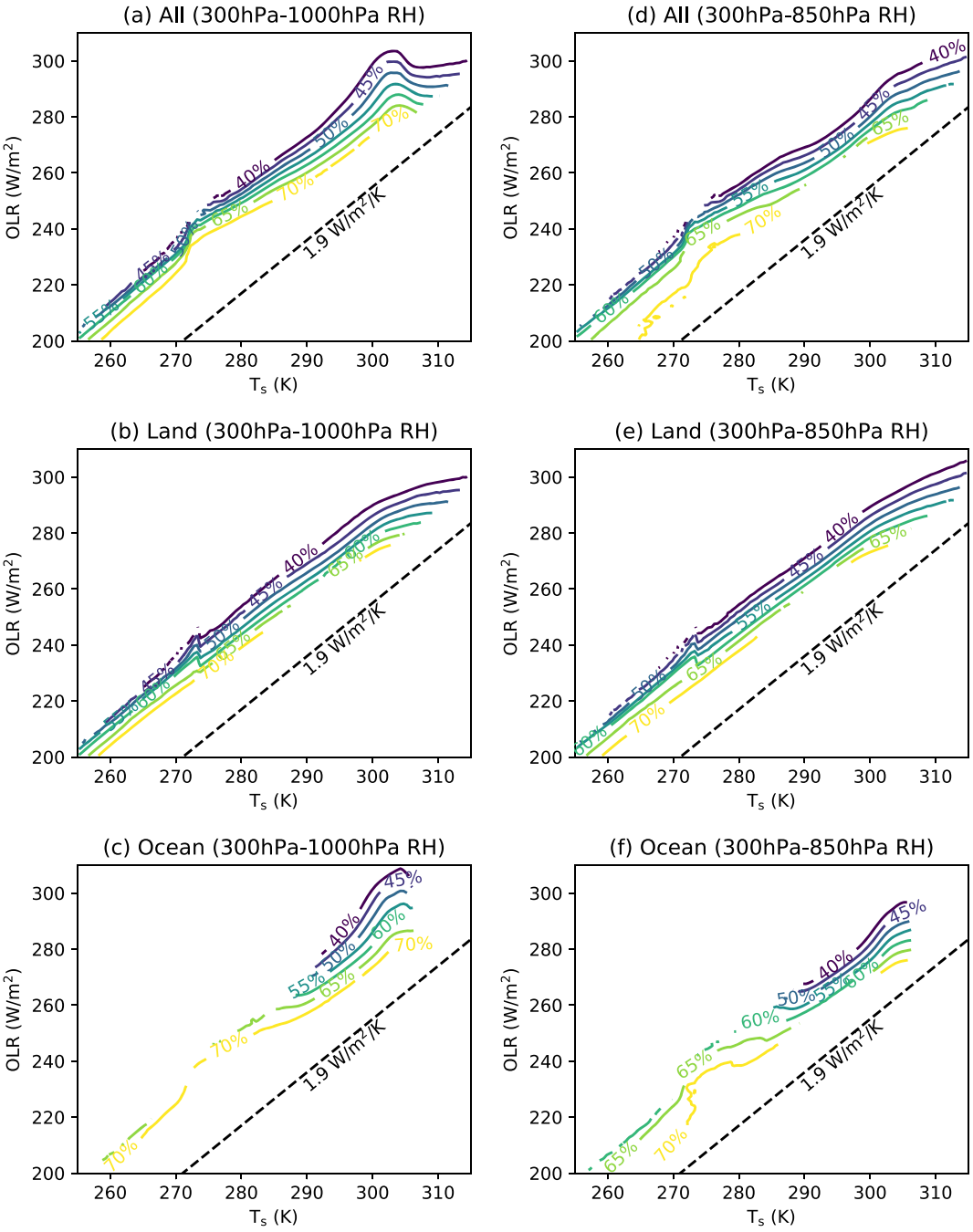

Figure 4. Clear-sky OLR versus surface temperature conditioned upon various column RH values. Data from nine CMIP5 models are included in the statistics. Column RH for 300–1,000 hPa is used for panels (a), (b), and (c), and column RH for 300–850 hPa (free troposphere) is used for panels (d), (e), and (f). Panels (a) and (d) include both land and ocean data, while panels (b) and (e) include land only, and panels (c) and (f) include ocean only. The dashed black line indicates a reference slope of 1.9 W/m^2/K.

Returning to the decrease of OLR with T_s at high T_s as shown in Figure 4a, we find that this decrease is caused by the transition from the lower T_s values populated by ocean regions to those higher T_s values populated by land regions. At fixed column RH, the boundary layer is dryer and the free troposphere is moister over land than over ocean. Thus, as one transitions from ocean to land columns at fixed column RH, one swaps boundary-layer moisture for free-tropospheric moisture. This reduces the OLR, leading to the kink

in Figure 4a at roughly 303 K. Indeed, land alone has a more linear OLR-T_s relationship (Figure 4b), though a mild decrease of OLR with T_s still exists for the warmest oceans (Figure 4c) located in between the subtropical deserts (e.g., the Red Sea) over which the boundary layer is very dry and more "land-like." Again, this decrease of OLR with T_s at fixed column RH is not the same as the super-greenhouse effect over tropical oceans, which stems from changing column RH as discussed in the previous section. Using free-tropospheric column RH, the land-ocean contrast is significantly reduced (Figures 4e and 4f) and the OLR-T_s relationship over land is simply an extension of that over ocean to higher T_s.

To summarize, despite the diversity of RH and temperature profiles in realistic climate models, the LWCS feedback (α) is indeed independent of both T_s and RH, consistent with Equation 1, so long as RH is interpreted as free-tropospheric column RH. Therefore, Equation 1 seems applicable to realistic atmospheres, and we can turn to the additional condition on column RH distribution.

5. Condition for Robust Global-Mean LWCS Feedback

Now we answer the question of under what conditions the compensation of local LWCS feedback seen in section 3 is guaranteed to produce a global-mean LWCS feedback around 2 $W/m^2/K$, consistent with Equation 1. In particular, we show that a sufficient condition is that the free-tropospheric column RH distribution, denoted $F(\mathrm{RH})$, stays invariant with global warming.

We denote the joint distribution of T_s and column RH as $f(T_s,\mathrm{RH})$, whose integral in T_s gives $F(\mathrm{RH})$. For convenience, we express the OLR in the following functional form, which is equivalent to Equation 1:

$$\mathrm{OLR}(T_s,\ \mathrm{RH}) = \alpha T_s + R(\mathrm{RH}), \tag{3}$$

where the specific functional form of $R(\mathrm{RH})$ is not of concern here. The global-mean clear-sky OLR ($\overline{\mathrm{OLR}}$) is thus

$$\overline{\mathrm{OLR}} = \int \mathrm{dRH} \int \mathrm{d}T_s f(T_s,\ \mathrm{RH})\mathrm{OLR}(T_s,\ \mathrm{RH}) \tag{4}$$

$$= \alpha \int \mathrm{dRH} \int \mathrm{d}T_s f(T_s,\ \mathrm{RH}) T_s + \int \mathrm{dRH} R(\mathrm{RH}) \int \mathrm{d}T_s f(T_s,\ \mathrm{RH}). \tag{5}$$

The integral in the first term of Equation 5 gives the global-mean surface temperature ($\overline{T_s}$), and the integral over T_s in the second term gives the column RH distribution; therefore

$$\overline{\mathrm{OLR}} = \alpha \overline{T_s} + \int \mathrm{dRH} R(\mathrm{RH}) F(\mathrm{RH}), \tag{6}$$

and thus

$$\delta\overline{\mathrm{OLR}} = \alpha \delta\overline{T_s} + \int \mathrm{dRH} R(\mathrm{RH}) \delta F(\mathrm{RH}). \tag{7}$$

If the column RH distribution remains constant with global warming, that is,

$$\delta F(\mathrm{RH}) \equiv 0, \tag{8}$$

then we have

$$\frac{\delta\overline{\mathrm{OLR}}}{\delta\overline{T_s}} = \alpha. \tag{9}$$

Therefore, the global-mean LWCS feedback is equal to the single-column LWCS feedback at constant RH (Equation 1 and Figure 4) so long as the global column RH histogram is invariant under global warming. Equation 9 is thus the global-mean analog for Equation 1, and Equation 8 is the global analog for the fixed-RH condition in the single-column model.

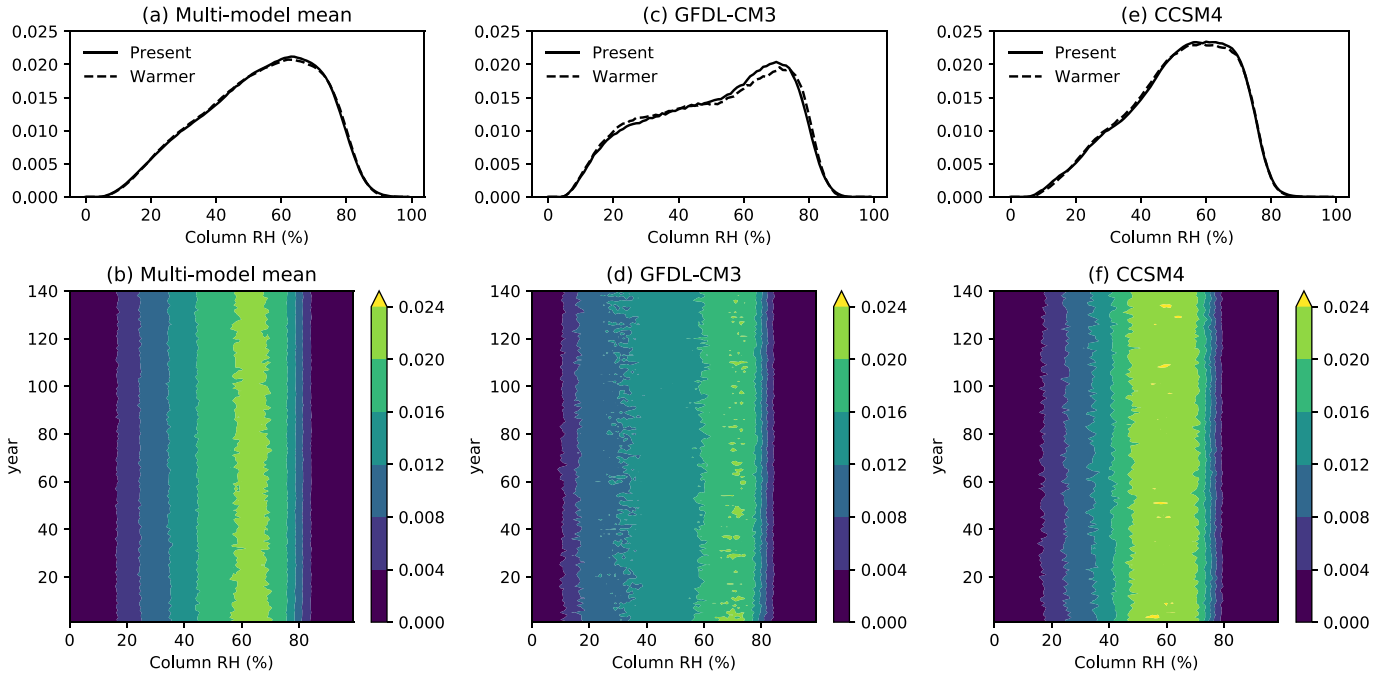

Figure 5. (a) The multimodel-mean histogram of free-tropospheric column RH in the first 10 years (solid; labeled "present") and the last 10 years (dashed; labeled "warmer") of the simulation. (b) Time series of the multimodel-mean free-tropospheric RH histogram throughout the simulation. (c) The same as panel (a) but for GFDL-CM3. (d) The same as panel (b) but for GFDL-CM3. (e) The same as panel (a) but for CCSM4. (f) The same as panel (b) but for CCSM4.

This additional condition, described by Equation 8, is indeed satisfied in CMIP5 models. Figure 5a shows that the multimodel mean histogram of free-tropospheric column RH is largely unchanged between the first and the last 10 years of the simulation, and the same is true for individual models (see Figures 5c and Figure 5e for GFDL-CM3 and CCSM4 as examples). Furthermore, this invariance holds on a year-to-year basis (Figures 5b, 5d, and 5f), which guarantees the linearity of global-mean OLR versus global-mean T_s for annual mean data as shown in Figure 1. This result is consistent with previous work that finds that the free tropospheric RH is overwhelmingly controlled by the large-scale circulation (Galewsky et al., 2005; Pierrehumbert & Roca, 1998; Sherwood & Meyer, 2006), and with the fact that constant free-tropospheric RH has long proved to be an accurate leading order assumption under global warming (Manabe & Wetherald, 1975). Note that these results are also true if boundary-layer RH is included in the column RH calculation (see Figure S1).

6. Summary

This paper aims to connect the idealized model results of Koll and Cronin (2018) to the behavior of comprehensive climate models, in line with the hierarchical approach to climate science (Held, 2005; Jeevanjee et al., 2017; Maher et al., 2019). In particular, we sought to understand whether the robustness of LWCS feedback in CMIP5 models could be traced back to the single-column physics of Koll and Cronin (2018). We found that indeed it could, on the condition that the global free-tropospheric column RH histogram remains invariant under warming. This invariance of the global RH histogram is a global analog of the fixed-RH condition for single-column models. In this sense, we have shown that "fixed RH" is a good approximation for the atmosphere under global warming, and the linearity of global-mean OLR is a direct consequence of this.

This invariance of the global column RH histogram is manifest in Figures 2a and 2c where a moistening of the deep tropics is accompanied by a drying of the subtropics. The super-greenhouse effect discussed in section 1 arises when this deep-tropical moistening is strong enough to make $\frac{\mathrm{dOLR}}{\mathrm{d}T_s}$ negative (see Equation 2). However, our results show that any such negative $\frac{\mathrm{dOLR}}{\mathrm{d}T_s}$ values must be offset elsewhere by

anomalously positive values. This means that, in a global or even a tropical-mean context, the clear-sky super-greenhouse effect is constrained to disappear (as evident in Figure 1) and thus has little impact on large-scale climate.

Data Availability Statement

CMIP5 model data can be accessed at https://esgf-node.llnl.gov/projects/cmip5.

Acknowledgments

N. J. thanks R. Pincus for feedback at an early stage of this work. Y. Z. acknowledges support under award NA18OAR4320123 from the National Oceanic and Atmospheric Administration, U.S. Department of Commerce. The statements, findings, conclusions, and recommendations are those of the author(s) and do not necessarily reflect the views of the National Oceanic and Atmospheric Administration or the U.S. Department of Commerce. S. F. acknowledges support from National Science Foundation Awards NSF PIRE-1743753 and AGS-1733818. We thank Daniel Koll for developing PyRADS code and making it publicly available (https://github.com/ddbkoll/PyRADS). We acknowledge the World Climate Research Programmes Working Group on Coupled Modelling, which is responsible for CMIP, and we thank the climate modeling groups (listed in Figure 1 of this paper) for producing and making available their model output. For CMIP, the U.S. Department of Energy's Program for Climate Model Diagnosis and Intercomparison provides coordinating support and led development of software infrastructure in partnership with the Global Organization for Earth System Science Portals.

References

Allan, R. P., Shine, K. P., Slingo, A., & Pamment, J. (1999). The dependence of clear-sky outgoing long-wave radiation on surface temperature and relative humidity. *Quarterly Journal of the Royal Meteorological Society*, *125*(558), 2103–2126.

Andrews, T., Gregory, J. M., & Webb, M. J. (2015). The dependence of radiative forcing and feedback on evolving patterns of surface temperature change in climate models. *Journal of Climate*, *28*(4), 1630–1648.

Byrne, M. P., & O'Gorman, P. A. (2016). Understanding decreases in land relative humidity with global warming: Conceptual model and GCM simulations. *Journal of Climate*, *29*(24), 9045–9061.

Dewey, M., & Goldblatt, C. (2018). Evidence for radiative-convective bistability in tropical atmospheres. *Geophysical Research Letters*, *45*, 10–673. https://doi.org/10.1029/2018GL078903

Feldl, N., & Roe, G. (2013). Four perspectives on climate feedbacks. *Geophysical Research Letters*, *40*, 4007–4011. https://doi.org/10.1002/grl.50711

Galewsky, J., Sobel, A., & Held, I. (2005). Diagnosis of subtropical humidity dynamics using tracers of last saturation. *Journal of the Atmospheric Sciences*, *62*(9), 3353–3367.

Gregory, J. M., Ingram, W. J., Palmer, M. A., Jones, G. S., Stott, P. A., Thorpe, R. B., & Williams, K. D. (2004). A new method for diagnosing radiative forcing and climate sensitivity. *Geophysical Research Letters*, *31*, L03205. https://doi.org/10.1029/2003GL018747

Held, I. M. (2005). The gap between simulation and understanding in climate modeling. *Bulletin of the American Meteorological Society*, *86*(11), 1609–1614.

Held, I. M., & Shell, K. M. (2012). Using relative humidity as a state variable in climate feedback analysis. *Journal of Climate*, *25*(8), 2578–2582. https://doi.org/10.1175/jcli-d-11-00721.1

Held, I. M., & Soden, B. J. (2000). Water vapor feedback and global warming. *Annual Review of Energy and the Environment*, *25*, 441–475. https://doi.org/10.1146/annurev.energy.25.1.441

Huang, Y., Ramaswamy, V., & Soden, B. (2007). An investigation of the sensitivity of the clear-sky outgoing longwave radiation to atmospheric temperature and water vapor. *Journal of Geophysical Research*, *112*, D05104. https://doi.org/10.1029/2005JD006906

Ingram, W. (2010). A very simple model for the water vapour feedback on climate change. *Journal of the Royal Meteorological Society: A Journal of the Atmospheric Sciences, Applied Meteorology and Physical Oceanography*, *136*(646), 30–40.

Jeevanjee, N., Hassanzadeh, P., Hill, S., & Sheshadri, A. (2017). A perspective on climate model hierarchies. *Journal of Advances in Modeling Earth Systems*, *9*(4), 1760–1771.

Koll, D. D., & Cronin, T. W. (2018). Earths outgoing longwave radiation linear due to H_2O greenhouse effect. *Proceedings of the National Academy of Sciences*, *115*(41), 10,293–10,298.

Maher, P., Gerber, E. P., Medeiros, B., Merlis, T. M., Sherwood, S., Sheshadri, A., & Zurita-Gotor, P.(2019). Model hierarchies for understanding atmospheric circulation. *Reviews of Geophysics*, *57*(2), 250–280.

Manabe, S., & Wetherald, R. T. (1975). The effects of doubling the CO_2 concentration on the climate of a general circulation model. *Journal of the Atmospheric Sciences*, *32*(1), 3–15.

Pierrehumbert, R. (1998). Lateral mixing as a source of subtropical water vapor. *Geophysical Research Letters*, *25*(2), 151–154.

Pierrehumbert, R. T., & Roca, R. (1998). Evidence for control of Atlantic subtropical humidity by large scale advection. *Geophysical Research Letters*, *25*(24), 4537–4540.

Raghuraman, S. P., Paynter, D., & Ramaswamy, V. (2019). Quantifying the drivers of the clear sky greenhouse effect, 2000–2016. *Journal of Geophysical Research: Atmospheres*, *124*, 11,354–11,371. https://doi.org/10.1029/2019JD031017

Raval, A., Oort, A., & Ramaswamy, V. (1994). Observed dependence of outgoing longwave radiation on sea surface temperature and moisture. *Journal of Climate*, *7*(5), 807–821.

Raval, A., & Ramanathan, V. (1989). Observational determination of the greenhouse effect. *Nature*, *342*(6251), 758–761.

Romps, D. M. (2014). An analytical model for tropical relative humidity. *Journal of Climate*, *27*(19), 7432–7449.

Sherwood, S. C., & Meyer, C. (2006). The general circulation and robust relative humidity. *Journal of Climate*, *19*, 6278–6279.

Shine, K. P., & Sinha, A. (1991). Sensitivity of the Earth's climate to height-dependent changes in the water vapour mixing ratio. *Nature*, *354*(6352), 382–384.

Soden, B., & Held, I. (2006). An assessment of climate feedbacks in coupled ocean-atmosphere models. *Journal of Climate*, *19*(2003), 3354–3360. https://doi.org/10.1175/JCLI9028.1

Soden, B. J., Held, I. M., Colman, R., Shell, K. M., Kiehl, J. T., & Shields, C. A. (2008). Quantifying climate feedbacks using radiative kernels. *Journal of Climate*, *21*(14), 3504–3520.

Stephens, G. L., & Greenwald, T. J. (1991). The Earth's radiation budget and its relation to atmospheric hydrology: 2. Observations of cloud effects. *Journal of Geophysical Research*, *96*(D8), 15,325–15,340.

Stephens, G. L., Kahn, B. H., & Richardson, M. (2016). The super greenhouse effect in a changing climate. *Journal of Climate*, *29*(15), 5469–5482.

Taylor, K. E., Stouffer, R. J., & Meehl, G. A. (2012). An overview of CMIP5 and the experiment design. *Bulletin of the American Meteorological Society*, *93*(4), 485–498.

Valero, F. P., Collins, W. D., Pilewskie, P., Bucholtz, A., & Flatau, P. J. (1997). Direct radiometric observations of the water vapor greenhouse effect over the equatorial Pacific Ocean. *Science*, *275*(5307), 1773–1776.